IET Circuits, Devices & Systems

Research Article

IET Journals
The Institution of Engineering and Technology

New oscillator concept based on band edge degeneracy in lumped double-ladder circuits

ISSN 1751-858X
Received on 28th March 2018
Revised 16th January 2019
Accepted on 8th February 2019
E-First on 1st July 2019
doi: 10.1049/iet-cds.2018.5048
www.ietdl.org

Dmitry Oshmarin[1], Farshad Yazdi[1], Mohamed A.K. Othman[1], Jeff Sloan[1], Mohammad Radfar[1], Michael M. Green[1], Filippo Capolino[1] ✉

[1]*Department of Electrical Engineering and Computer Science, University of California, Irvine, CA 92697, USA*
✉ *E-mail: f.capolino@uci.edu*

Abstract: An oscillator scheme based on the degenerate band edge (DBE) in a periodic, double-ladder resonant circuit made of lumped elements is proposed for the first time. The circuit exhibits a DBE in the dispersion diagram of its phase-frequency eigenstates and possesses unique resonance features associated with a high loaded *Q*-factor resonance, compared to a single-ladder circuit. This oscillator is shown to have an oscillation threshold that is half that of a single LC ladder circuit having the same total quality factor, and thus is more robust than an LC oscillator in the presence of losses. Moreover, the double-ladder oscillators have a unique mode selection scheme that leads to stable single-frequency oscillations even when the load is varied. It is also shown that the output amplitude of the double-ladder oscillator is much less sensitive to the output loading compared to single-ladder oscillators. The authors show the analysis and design of such oscillators that potentially lead to enhancing the efficiency of RF components and sources.

1 Introduction

Oscillators are essential components of any radio frequency (RF) system. Typically, an RF oscillator operates via a positive feedback mechanism utilising a gain device with a selective reactive circuit that generates a single tone used as the carrier frequency. The most common oscillator configuration is based on an LC tank [1–4]. The negative resistance required for positive feedback can be obtained from topologies such as Pierce, Colpitts, and Gunn diode waveguide oscillators, as well as a cross-coupled transistor pair [3, 5–7]. While widely used, all designs based on an LC-tank circuit have some important limitations; their performance largely depends on the loading conditions as well as the need for active buffers. While oscillator based on LC tank is the most common, other designs may feature distributed [8, 9], ring [10, 11], coupled [12], or multi-mode [13] oscillators which come with their own set of challenges.

The focus of this paper is on the latter; to propose a new oscillator concept based on degeneracy condition as explained in Section 2. The proposed oscillator is called the 'double-ladder oscillator' and it utilises the degenerate band edge (DBE) property that exists in a circuit made of cascaded unit cells, each consisting of reactive components.

Some of the potential advantages of the double-ladder circuit are that its criteria for oscillation are more relaxed, its oscillation frequency is independent of loading, and it does not need active output buffer stages for the load termination. Furthermore, while the design presented here utilises lumped elements, all of the introduced oscillator concepts can be easily applied to different implementations since the DBE has already been demonstrated in microstrip [14, 15] and circular waveguide [16, 17] technologies. While electron-beam-based oscillators and lasers schemes based on the DBE phenomenon have been shown very recently in [18] and [19], respectively, the new radio frequency oscillator regime based on lumped element ladder circuit with DBE is presented here for the first time. A major benefit of the lumped circuit approach is the simplicity of the DBE oscillator design. This simplicity is manifested in the comprehensive understanding of its behaviour and how it can be suitable to improving oscillator design. Furthermore, the lumped circuit double ladder considered in this manuscript mimics the distributed model of transmission lines (TL). Therefore, the lumped element circuit gives an accurate representation of a potential TL design by means of precise time domain simulations without an actual realisation of a TL circuit. Furthermore, in some cases, it is convenient to perform the time domain analysis of TLs by approximating distributed elements with lumped element circuits; therefore, these findings provide a direct path to understanding TL-based DBE oscillators, which is a topic for future research. The basic properties of the DBE are shown in [20] when realised with lumped elements, in [21, 22] when realised using multilayer environments and in [23] when realised using TLs.

In Section 2, a brief description of the properties of single- and double-ladder circuits is provided. In Section 3, the resonance characteristics, including the effect of losses on the double ladder, are explored. In Section 4, we analyse the threshold conditions for oscillation by a negative differential resistance. In Section 5, we investigate time-domain behaviour of the oscillators that includes the active device non-linearity. In Sections 2, 3, and 4, we assume that the circuits are operating in the sinusoidal steady state so that all voltages and currents are represented by phasors.

2 Single- and double-ladder circuits

2.1 Single-ladder circuit

We consider a periodic resonant circuit made up of LC ladder cells connected in tandem. A simple example of such a cell, comprising a series inductor and a shunt capacitor, is shown in Fig. 1*a*. Finite-length implementations of periodic circuits have many applications including filters, pulse-shaping networks, and delay lines [24–26].

Let us now suppose that Fig. 1*a* ladder of infinite length is excited by a sinusoidal source with frequency ω, and is operating in steady state. For this mode of operation, all of the currents and voltages can be expressed as phasors; in particular, the phasor ratio $V_1(n+1)/V_1(n)$ can be determined by simply finding the eigenvalues and eigenvectors of the transmission matrix describing the unit cell (note that these eigenvalues are not the same as the circuit's natural frequencies; see Ch. 8 in [27]). Moreover, it can be shown that for sufficiently low angular frequency ω, $V_1(n+1)/V_1(n)$ has unity magnitude; i.e. all voltages and currents have the same amplitude, differing only by a fixed phase shift $\varphi(\omega)$. Therefore, we define the eigenstates for a periodic circuit as the possible solutions of the eigenvalue problem describing the

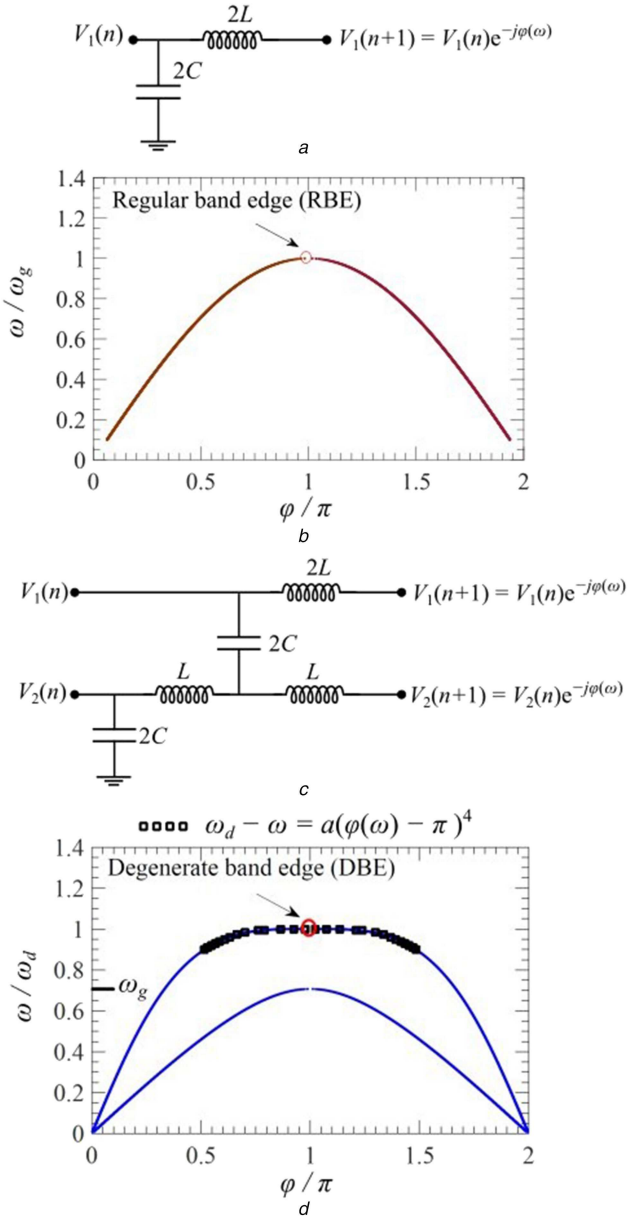

Fig. 1 *Basic unit cell geometries and their dispersion relation*
(a) Unit cell of a periodic single-ladder lumped circuit, ***(b)*** Dispersion diagram, real phase shift versus frequency, of the periodic single-ladder circuit that develops an RBE at an angular frequency ω_g, ***(c)*** Unit cell of a periodic double-ladder lumped circuit, ***(d)*** Dispersion diagram of the periodic double-ladder circuit that develops a DBE at an angular frequency ω_d. Also, the asymptotic dispersion relation typical of DBE, $\omega - \omega_d = a[\varphi - \pi]^4$, is plotted as square symbols

evolution of the voltages and currents from one cell to the next in the periodic circuit following the Bloch–Floquet theory (see Ch. 8 in [27], and also [28]). In general, each eigenstate is characterised by voltages and currents that vary from cell to cell as $\exp(-j\gamma)$, where $\gamma = \varphi - j\alpha$ is the complex phase shift from one unit cell to the next.

The relation between the applied frequency and the phase shift between cells in an infinitely long periodic ladder is known as the *dispersion relation*. For the 'single' ladder in Fig. 1*a*, it can be shown that the eigenvalues of the transfer matrix [20, 27] are given by

$$e^{-j\gamma} = 1 - 2\left(\frac{\omega}{\omega_g}\right)^2 \pm 2\frac{\omega}{\omega_g}\sqrt{\left(\frac{\omega}{\omega_g}\right)^2 - 1} \tag{1}$$

where $\omega_g = \sqrt{1/(LC)}$. For $\omega = \omega_g$, these two eigenvalues coalesce and have unity magnitude at which $\gamma = \varphi = \pi$ and $\alpha = 0$. The corresponding dispersion relation is shown in the curve labelled regular band edge (RBE) in Fig. 1*b* at $\omega_g = \sqrt{1/(LC)}$. The dispersion of these states of phase near $\omega = \omega_g$ behaves as $(\omega_g - \omega) \propto (\gamma - \pi)^2$. (In this curve the range of principal values of the inverse tangent function used to obtain $\varphi(\omega)$ is chosen to be from 0 to 2π, and only the dispersion of eigenstates for which $\alpha = 0$ are plotted in a conventional manner [27]). The frequency ω_g, known as the *band edge*, defines the passband for the periodic circuit. At frequencies higher than ω_g, the eigenvalues will no longer have unity magnitude, and thus $V_1(n+1)/V_1(n)$ will have both an attenuation factor and a phase shift. This range of frequencies corresponds to the stopband, and the condition is known as an evanescent state.

Note that in Fig. 1*b* at $\omega = \omega_g$, the two phase shifts corresponding to the eigenvalues in (1) coalesce into a single value. This phenomenon is well-known in periodic structures that naturally exhibit an electromagnetic band gap [27]. In general, periodic structures composed of TLs or waveguides have been shown to demonstrate unique properties associated with 'slow-light' properties near the band edge [27–29]. Such properties are associated with very high group delay near the band edge and consequently lead to enhancing the quality factor of resonators. Several applications have been investigated in lasers and high-power electron beam devices based on the band-edge operation [29–32].

2.2 Double-Ladder circuit

We now consider a periodic double-ladder circuit whose unit cell with four ports is shown in Fig. 1*c*. Since each unit cell is a grounded four-port network, this circuit supports four eigenstates rather than two, as was the case for the unit cell in Fig. 1*a* [7, 21]. Under an appropriate choice of the circuit elements, at a certain frequency, these four eigenstates coalesce at $\varphi = \pi$ and $\alpha = 0$ resulting in the so-called DBE condition [15, 16, 22, 33]. The four sets of voltage and currents associated with these eigenstates are no longer independent at this degeneracy point [20]. A DBE can only be found in double ladders since it represents the degeneracy of four eigenstates [20]. Near the DBE condition, the phase-frequency dispersion relation of these states is characterised by $(\omega_d - \omega) \approx a(\gamma - \pi)^4$ where a is a geometry-dependent fitting constant, whose analytic expression is given in [20]. It is also worth noting that the above relation is exactly satisfied at $\omega/\omega_d = 1$, there providing the exact normalised complex phase shift $\gamma/\pi = 1$, and almost nearly satisfied for a wide range of complex phase shift γ/π values in the vicinity of 1, because of the quartic dependence, as seen in Fig. 1*d*. This property *is not* shared by the RBE as seen in Fig. 1*b*, where at $\omega/\omega_g = 1$, the frequency dispersion relation $\Delta\omega/\omega_g \propto (\Delta\gamma/\pi)^2$ is exactly satisfied, but almost nearly satisfied for a much smaller range of γ/π values than for the DBE case. This provides some tolerance against perturbations of the circuit elements in determining the resonance frequency. The study of how tolerant the circuit is to those perturbations will be carried out in the future as the main focus of this paper is the introduction to the new DBE oscillator concept and its basic operation principles.

For the unit cell shown in Fig. 1*c*, the DBE angular frequency is given by $\omega_d = 1/\sqrt{LC}$, while the characteristic impedance is $Z_c = \sqrt{L/C}$ [20]. The theory of lumped circuits with DBE has been developed in [20], where different double-ladder circuit configurations composed of cascaded identical unit cells are studied. The normalised dispersion diagram for the four-port periodic circuit with the proposed unit cell is depicted in Fig. 1*d*. Note that the circuit in Fig. 1*c* exhibits an RBE, as well, at an angular frequency $\omega_g = \omega_d/\sqrt{2}$ for the double ladder, at which two of the eigenstates coalesce similar to the dispersion of a single LC ladder. However, at $\omega = \omega_d$, a DBE, where all four states coalesce, can be observed. For the circuit in Fig. 1*c,* a value of $a = 120\ \mathrm{s}^{-1}$ was used to fit the curve in Fig. 1*d*. To provide a practical implementation at RF, values for the lumped capacitors and inductors are chosen from commercially available lumped elements

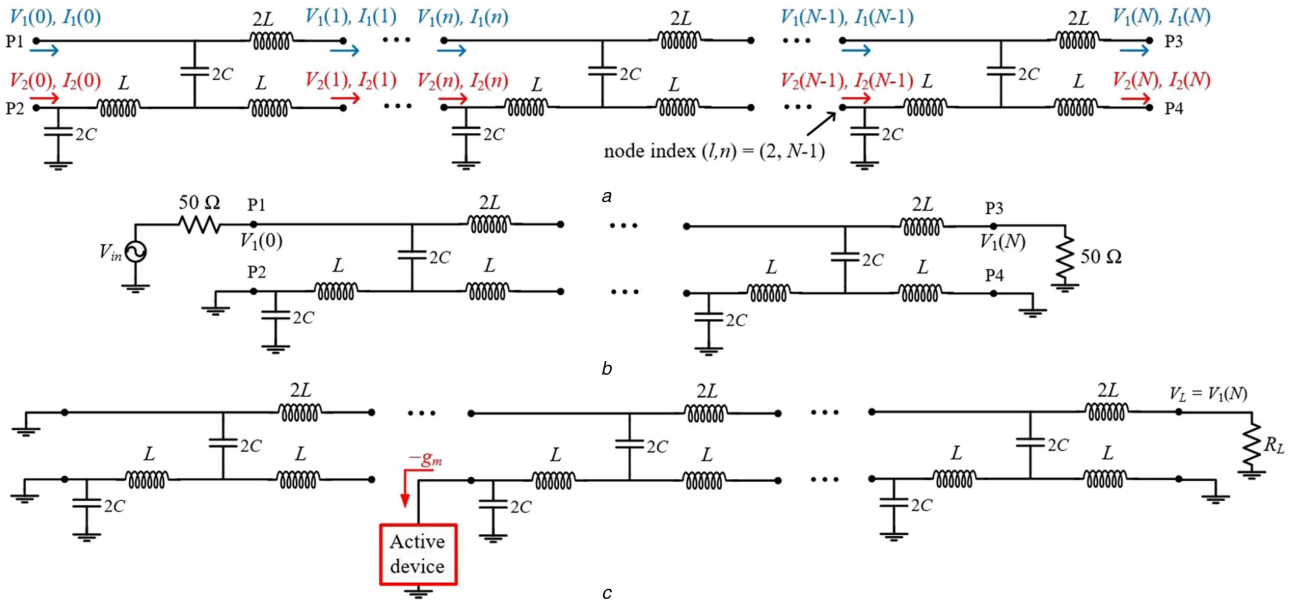

Fig. 2 *Periodic arrangement of unit cells of Fig. 1(c)*

(a) Double LC ladder periodic circuit made of N unit cells operated near the DBE. P1 through P4 represent the four ports of the N-cell circuit, ***(b)*** circuit with excitation voltage V_{in} and source resistance of 50, and 50 Ω load at P3, ***(c)*** double-ladder oscillator with terminations and active device configuration (other configurations may have an active device in each unit cell)

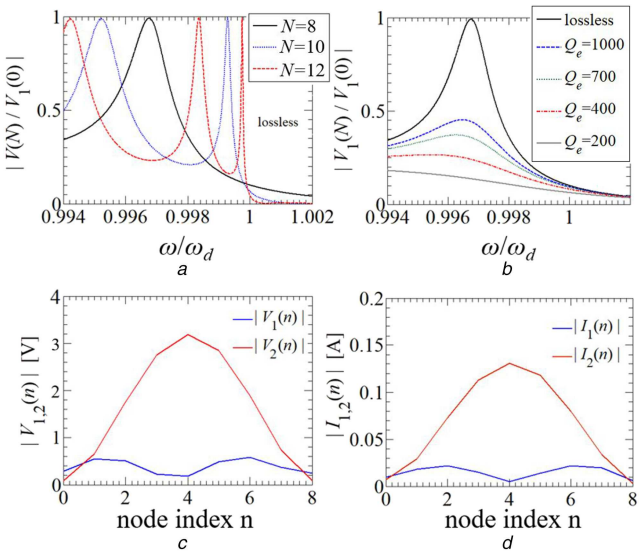

Fig. 3 *Voltage transfer function between the upper output P3 and upper input P1 nodes of the circuit with terminations as shown in Figs. 2b for*

(a) Different number of unit cells and no loss in the elements and, ***(b)*** Different quality factors for elements in an 8 unit cells resonator. The important resonance is the one close to ω_d, denoted as $\omega_{r,d}$, ***(c)*** Voltage distribution corresponding to $Q_e = 200$ in the upper ladder nodes and the lower ladder nodes of the circuit composed of 8 unit cells at the DBE resonance occurring at $\omega_{r,\mathrm{d}}$, ***(d)*** Current distribution in the upper ladder nodes and the lower nodes of the circuit composed of 8 unit cells

whose Q_e factor can exceed 200 [34, 35]. Namely, the following ladder circuits are composed of inductors and capacitors whose values are $L = 45$ nH and $C = 56$ pF, respectively. As a result, the circuit has a DBE frequency $f_d = 1/(2\pi\sqrt{LC}) \cong 100.26$ MHz and $Z_c = 28.3$ Ω.

3 Resonances of passive double-ladder circuit

In this section, we consider double-ladder circuits as shown in Fig. 2*a* made by cascading a finite number N of unit cells shown in Fig. 1*c*, and analyse their resonance characteristics related to the DBE. In particular, we first investigate important characteristics of passive double-ladder circuits, for which the effects of element losses on the transfer functions, loaded quality factor, and driving point admittance are explored in detail. These particular features allow for an unconventional way to construct oscillators. We also compare the double-ladder and single-ladder oscillators, while highlighting the advantages of the former and demonstrating that single-ladder oscillators can operate with multiple resonant modes and thus can generate multiple frequencies, while double-ladder oscillators can only oscillate at a single frequency.

Another undesirable property of the single-ladder configuration is mode jumping, in which the frequency of oscillation can change with the load resistance, as reported in the literature [13]. However, here we demonstrate that double-ladder oscillators are not prone to load-dependent variations, thereby exhibiting a more stable oscillation frequency and lower threshold for oscillation as compared to a single-ladder implementation.

As shown in Fig. 2*a*, every unit cell has four terminal nodes, each of which is identified by two indices: $l \in \{1, 2\}$ denoting the upper or lower ladder, respectively, and $n \in \{0, 1, 2, \ldots, N\}$ denoting the node location along the double ladder. As such, each cell's terminal nodes in Fig. 2*a* ladder will be referred to using the notation (l, n). When a double-ladder circuit composed of N cells is terminated at both ends by resistive loads, there will be a number of complex-valued natural frequencies, corresponding to resonance modes. It can be shown that the resonance angular frequencies associated to the peaks in Fig. 3*a* are approximated by $\omega_d - \omega_{r,m} \approx a(m/N)^4$ near the DBE angular frequency ω_d where m is a positive integer designating the resonance mode (similar to other periodic structures with DBE in [18, 22, 36]). We focus here on the closest resonance to the DBE corresponding to $m = 1$ with angular frequency $\omega_{r,1}$, since it retains most of the properties associated with the DBE; consequently, it is the sharpest one and provides a 'giant' resonance as explained in [22]. To be consistent with [20], we will refer to this frequency as $\omega_{r,\mathrm{d}}$ throughout the rest of this paper.

Characteristics of the DBE resonator have been discussed thoroughly in [16–20, 23] and in particular double-ladder lossless circuit properties have been shown in depth in [20]. Instead, here we focus on the effect of losses on the performance of the DBE resonator and how they are related to threshold criteria for oscillation and the performance of DBE-based oscillators in general.

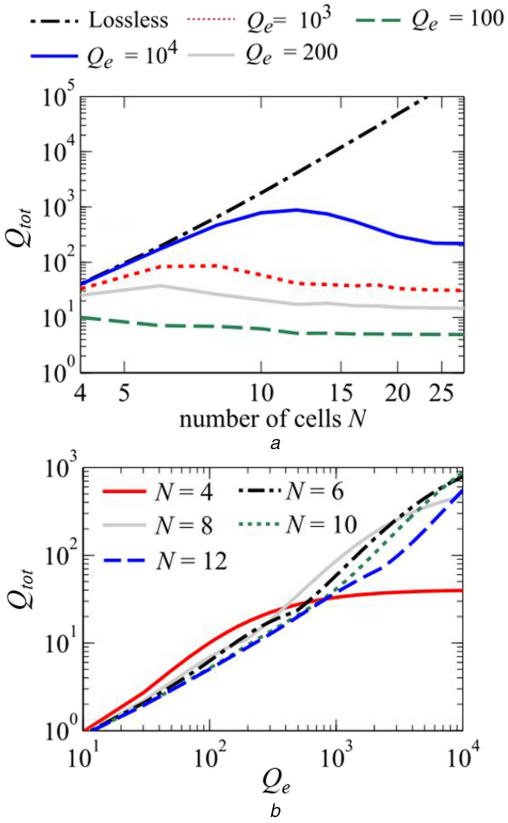

Fig. 4 *Loaded quality factor scaling versus*
(a) Number of unit cells N for different element quality, as well as for the lossless theoretical limit, ***(b)*** Element quality factor Q_e for different number of unit cells

3.1 Transfer function

As mentioned in the previous Section, the DBE resonance mode is associated with an excitation of all four eigenstates [22, 33, 36]. In this Section, we assume, as shown in Fig. 2*b*, that the double ladder is terminated with a 50 Ω load at port 3, and with a voltage source V_{in} in series with 50 Ω at port 1. The lower ladder is shorted to ground at ports 2 and 4. We first calculate the voltage transfer function, $|V_1(N)/V_1(0)|$, of this circuit for frequencies near the DBE, for $N = 8$, 10, and 12; the magnitudes of these transfer functions are shown in Fig. 3*a*. As shown in [20], the DBE-related transmission resonance peak at $\omega_{r,d}$ in the double-ladder circuit exhibits the highest Q among the other resonances, and its quality factor has been shown to scale as N^5 [20]. As noted previously [33], the group delay near the DBE is very large as can be observed by the flat region of the dispersion diagram in Fig. 1*d*, which corresponds to a high-quality factor even when the circuit is terminated by its characteristic impedance. (This impedance is the result of the chosen L and C for oscillation frequency at 100 MHz, as described in Section 2.2). Furthermore, as can be seen from Fig. 3*a*, by increasing the number of unit cells, the DBE resonance frequency $\omega_{r,d}$ approaches the DBE frequency ω_d. However, when losses are introduced into each L and C in the circuit, the resonance-loaded quality factor at $\omega_{r,d}$ is significantly reduced as compared to other resonances of the circuit. In Fig. 3*b*, the transfer function of the double-ladder circuit is depicted only for the resonance closest to the DBE for $N = 8$. For simplicity, it is assumed that all elements have the same quality factor Q_e.

Figs. 3*c* and *d* show how voltage and current magnitudes at the frequency $\omega_{r,d}$ vary throughout the circuit for $Q_e = 200$. These voltages and currents are evaluated at the nth node, $n = 0, 1, \ldots 8$, in the finite double-ladder circuit in Fig. 2*b*. In Fig. 3*c*, the voltage distributions on the lower TL (red) and the upper TL (blue) are depicted; likewise, in Fig. 3*d*, the current distributions for the upper and lower lines are plotted. It is interesting to note that both the voltage and current reach their peak magnitudes in the middle of the lower ladder; these magnitudes are approximately six times larger than those of the upper ladder, even when losses are present. On one hand, the reason for excitation of such voltage and current in the resonator is due to the excitation of all of the eigenstates of the periodic double ladder near the DBE condition, which is a general property of DBE resonators [18, 22, 33, 36]. On the other hand, the eigenstates of such particular periodic ladders have a voltage distribution that is mostly confined to the lower ladder, in the sense that the upper ladder nodes are essentially RF grounds; this is also true of the middle node in the lower ladder (node with $l = 2$, $n = 4$) [20]. The same behaviour can be seen for the current distribution as well. Therefore, most of the energy stored in the resonator is confined in the lower ladder's components. As can be seen from the voltage distribution inside the eight-cell structure shown in Figs. 3*c* and *d*, the maximum voltage amplitude occurs in the middle of the structure, while the voltage is attenuated by an order of magnitude at the edges. Since the load resistor is connected at one of these edges, its value will not have a substantial effect on the circuit's oscillation behaviour. Note that the voltage amplitude in the middle is quite high (3 V), due to the DBE effect. As a result, the presented oscillator will require less DC power, as compared to an LC tank with an active buffer, even though the eight-cell structure has many more lossy elements.

3.2 Total quality factor

To provide a comprehensive analysis of the performance of the lossy resonator, we calculate the loaded quality factor Q_{tot} of the double ladder – that is, the quality factor of the circuit including the resistive port terminations as well as the losses in the L and C components. This loaded quality factor associated with the resonance $\omega_{r,d}$ is defined as [27]

$$Q_{\text{tot}} = \omega_{r,d}\frac{W_e + W_m}{P_l} \tag{2}$$

where W_e and W_m are the total time-average energy stored in the circuits in the capacitors and inductors, respectively, and P_l is the time-average power dissipated in the resistive terminations and in the components' loss. In [20], the loaded quality factor of a lossless double ladder is thoroughly analysed, and instead the focus here is the effect of component losses on Q_{tot}. For this circuit and for other structures with DBE [17, 33, 37] and without losses, Q_{tot} is proportional to N^5 for large N as shown in [20]. Fig. 4 shows how the loaded quality factor scales with number of unit cells N and lumped element's quality factor Q_e, showing that for a realistic Q_e, of around 200 as chosen in this paper, eight unit cells is the optimal number to have a good Q_{tot}.

As can be seen from the phase noise formulation in [38–40], phase noise is a function of the inverse of the loaded quality factor Q_{tot}, among other parameters such as resonant frequency and power of the signal. All oscillators suffer from phase and amplitude perturbations, phase being the more prevailing of the two since the amplitude has an inherent stabilisation due to loop gain [38]. Thus, a design with inherent high Q_{tot}, such as ours, allows for natural reduction of the phase noise. The precise role of the $(\omega_d - \omega) \approx a(\gamma - \pi)^4$ dispersion flatness on phase noise at $\omega \approx \omega_d$ has yet to be studied. Since the goal of this paper was the introduction of the new concept of the DBE oscillator, the detailed phase noise analysis is left for the future studies where an in-depth comparison with a single ladder and an LC tank will be performed.

3.3 Driving point admittance Yin

The most important characteristic for estimating the oscillation criteria is the driving-point impedance at the location where an active device will be connected in order to start the oscillation [2]. As of the very large resonance voltage and current in the lower ladder relative to the DBE as seen in Fig. 3*c*, driving the lower ladder, especially near the middle of the resonator at the node denoted by $(l,n) = (2, N/2)$ with a negative conductance, would have the greatest impact in compensating the effect of losses in the circuit to achieve oscillation. Note that in other circuit

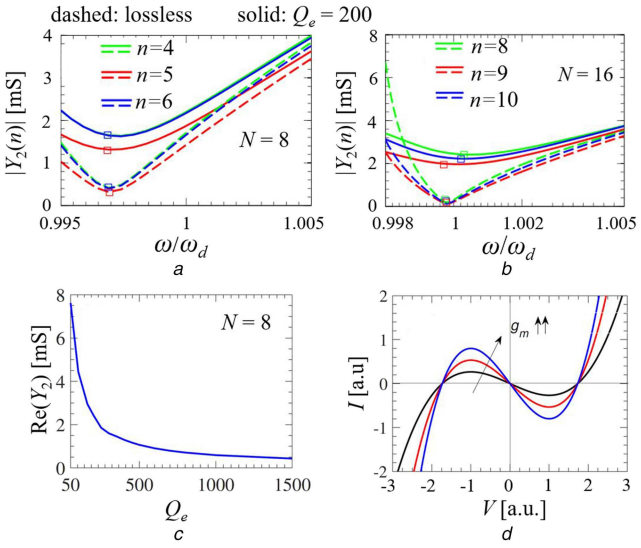

Fig. 5 *Magnitude of admittance near the DBE throughout the different nodes of the double ladder circuit for*

(a) $N = 8$ unit cells and ***(b)*** $N = 16$ unit cells. Square symbols denote the resonance frequency at which $\mathrm{Im}(Y_2(n)) = 0$, ***(c)*** magnitude of the driving point admittance at the resonance frequency versus quality factor of elements for $N = 8$ cell double ladder resonator, ***(d)*** Characteristic for the active device $I = -g_m V + \zeta V^3$ in which $\zeta = g_m/(3V_b^2)$, that exhibits small-signal negative resistance

configurations, the same analysis is necessary to predict the location of the peak voltage and consequently the driving point.

To provide a meaningful assessment of the oscillation threshold, we consider a single-ended loading scheme in which port 3 is terminated by 50 Ω load, while ports 1, 2, and 4 are terminated by a short circuit as shown in Fig. 2*c*.

In Figs. 5*a* and *b,* we show the magnitude of the driving-point admittance versus normalised frequency at the three middle nodes of the circuit for $N = 8$ and $N = 16$ unit cells (i.e. nodes $n = 4$, 5, 6 and $n = 8$, 9, 10, respectively, with $l = 2$). Both lossless and lossy elements with $Q_e = 200$ are considered. From the results shown in Figs. 5*a* and *b,* it can be seen that the lower ladder's node in the 5th and 9th unit cell, corresponding to $N = 8$ and $N = 16$, respectively, exhibit the lowest input admittances; thus they constitute the appropriate driving points for both configurations. It can also be seen from Figs. 5*a* and *b* that as the number of cells increases, the trend for the input admittance is different for the lossy and lossless circuits.

When N increases from 8 to 16, the admittance decreases by 50% for the lossless case (dashed lines in Figs. 5*a* and *b*), while it increases by 40% for the case with $Q_e = 200$ (solid lines). (Note that the minimum value of the admittance's magnitude does not exactly correspond to the resonance condition at which $\mathrm{Im}(Y_{\mathrm{in}}) = 0$); the resonance frequency is indicated in Figs. 5*a* and *b* with a square symbol.

To realise an oscillator, we use the circuit shown in Fig. 2*c*, which shows all of the port terminations and the placement of the active device, and plot the real part of the input admittance at resonance for an eight-cell double-ladder circuit as a function of the loaded quality factor of elements, shown in Fig. 5*c*. It can be observed that the admittance rapidly decreases as Q_e increases, and saturates after some value (for $Q_e < 2000$, we have $\mathrm{Re}(Y_2) = 0.2$ mS). Thus, selecting elements with very high Q_e is not necessary when constructing an oscillator since the applied negative resistance value required for oscillation will only be slightly higher in magnitude. (To compare these characteristics with those of a single LC ladder filters, we refer the reader to [13, 25, 26] for filtering characteristics of a single ladder, as well as for the scaling of the quality factor of regular band edge resonators).

It is very important to point out the DBE oscillator could operate in two different ways. One would be by applying an active device to each unit cell. This could be done by using a set of differential cross-coupled pairs, for instance. Thus, working near the DBE would not only provide for good conditions for the driving point admittance but would also provide nearly 180° phase shift from one cell to the next such that a cross-coupled pair between two cells would guarantee fully differential operation. The other way would be to connect just one single-ended active device (such as those in [2, 41], for example) which we investigate next.

4 Active double ladder circuit

In this section, we investigate the oscillation condition of the double-ladder circuit and compare some of the important characteristics of oscillations of the proposed double-ladder oscillator to a single-ladder-based oscillator. For purposes of the comparison, we will use the same number of cells in both structures. The proposed oscillator is composed of a double ladder terminated by a single-ended resistive load in the upper ladder end as seen in Fig. 2*c* (as described in Section 2.2), while the active device (a single-ended negative resistance) is attached to the driving point. As in most LC-based oscillators, the conditions for oscillation are formulated using the Barkhausen criteria for the feedback system [3, 42].

An active device used to induce oscillations can be characterised by its operating *I-V* curves. A negative resistance can be practically implemented by CMOS transistors or diodes and an example for a third-order *I-V* characteristic is shown in Fig. 5*d*, which utilises the following equation:

$$I = -g_m V + \zeta V^3, \tag{3}$$

where $-g_m$ is the slope of the *I-V* curve in the negative resistance region, and ζ is the third-order non-linearity constant that models the turning points of the characteristic. (It is this characteristic that determines the steady-state oscillation amplitude.) To realise a constant DC voltage-biased active device, we choose the turning point V_b of the *I-V* characteristics to be constant under different biasing levels. In particular, we set $\zeta = g_m/(3V_b^2)$, as shown in Fig. 5*d*. We also assume that the capacitances in the ladder are much larger than any parasitic capacitance associated with the negative resistance device. Calculations are carried out using ADS transient solver.

4.1 Transconductance parametrisation

As previously discussed, the negative conductance required to cancel losses, thereby allowing oscillations to start up, is to measure the driving-point admittance at the port where this conductance will be inserted. From Fig. 5*a*, Y_{in} of the 5th cell is ~1.2 mS. Fig. 6*a* shows the minimum magnitude of the transconductance versus the number of cells of the double ladder.

The lossless double ladder's threshold follows the same trend as its quality factor varying as a function of length; i.e. since $Q_{\mathrm{tot}} \propto N^5$ the double ladder's threshold $g_{m,\min} \propto 1/N^5$ when the active device is attached to every cell. In addition, it can be observed that when the active device is connected only to the middle cell, the threshold is higher and its trend versus N is fitted to $g_{m,\min} \propto 1/N^{3.75}$. This is a remarkable feature of DBE resonators in general as compared to single-ladder oscillators in which scaling is $g_{m,\min} \propto 1/N^3$ when active devices are connected to *each* cell [16]. When element losses are considered here with $Q_{\mathrm{e}} = 200$, the minimum g_m increases from the lossless case, particularly for large N. However, we see that for large N, the threshold saturates, which is a consequence of the saturation feature of Q_{tot} factor versus Q_e.

To provide a meaningful comparison, we compare the threshold $g_{m,\min}$ at the $(l,n) = (2, N/2)$ node cell only, varying as a function of the Q_e as well as Q_{tot}. For all of the remaining simulations, the driving point for negative resistance is set to be the $(N/2 + 1)$th cell. It is shown in Fig. 6*b* that for a given Q_{tot}, the double-ladder exhibits a lower oscillation threshold than the single ladder.

Moreover, when comparing the threshold versus the element Q_{e}, the double ladder shows a lower threshold even for a relatively low element $Q_{\mathrm{e}} < 100$. The reason for the better behaviour of the

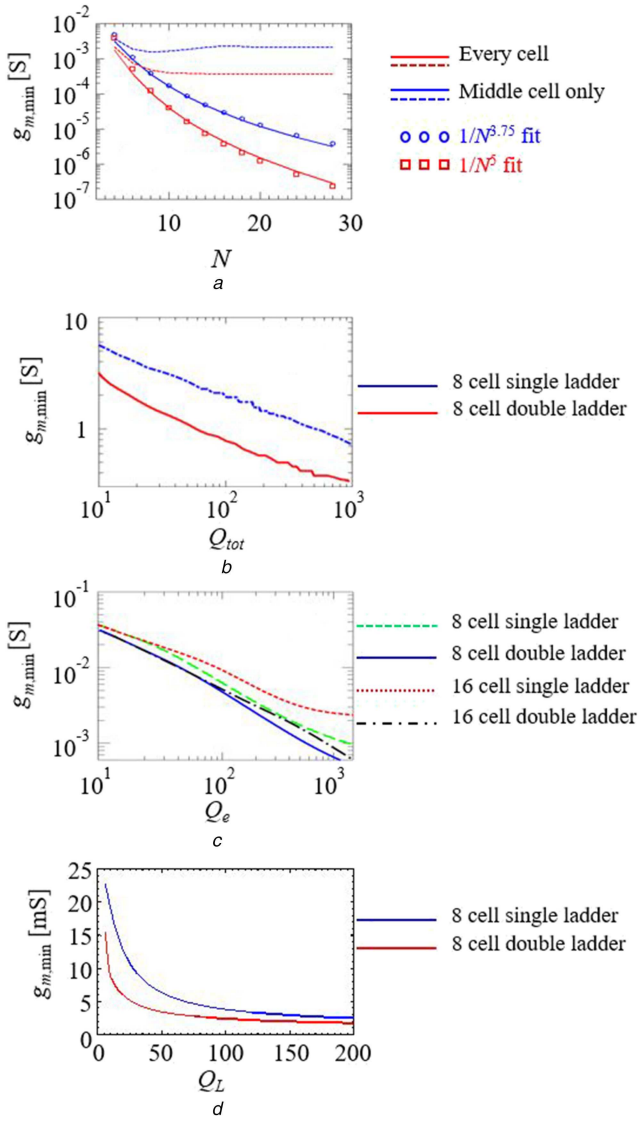

Fig. 6 *Minimum g_m, $g_{m,min}$, (to start oscillations) scaling versus*
(a) Number of unit cells N for the double-ladder oscillator. The plot also shows for the lossless case a trend corresponding to $g_{m,\min} \propto 1/N^5$, ***(b)*** Different values for loaded quality factor Q_{tot}, ***(c)*** Lumped element quality factor, Qe, for double ladders and single ladders of two different sizes $N = 8$ and $N = 16$, ***(d)*** Inductor quality factor Q_L for double and single ladders with eight unit cells (all the other Qs and load are kept constant). In all of cases the threshold of the double ladder is lower than that of the single ladder

double ladder is that it features a fourth-order degeneracy. Fig. 6*c* shows how the threshold transconductance varies as a function of Q_e for a double ladder and single ladder of two different sizes with $N = 8$ and $N = 16$ unit cells. We can see that for a low element quality factor, the eight-cell double-ladder circuit has the lowest threshold, for $Q_e > 100$. Furthermore, the single ladder of 16 cells has a higher threshold than all other configurations, which indicates that a double ladder has an improved characteristic compared to a single ladder. This is a novel phenomenon that could be further investigated in order to enhance the efficiency of microwave oscillators. Fig. 6*d* shows threshold transconductance versus inductor quality factor, Q_L, while keeping capacitor Q_e of 460 unchanged from the previously reported value. Realistic values of inductor Q_L drop rapidly as frequency of operation increases, especially in integrated circuits technology, but even at low Q_L values, above ~5 (below which oscillation does not happen), DBE oscillators based on double ladder demonstrates 75% lower threshold than RBE oscillators based on single ladder, up to Q_L of 50. This remarkable property is again due to the DBE phenomena and its ability to have a higher Q_{tot} even with low element Q's.

5 Double-Ladder oscillator

In this section, we study the time-domain response of the proposed double-ladder oscillator (DLO), as well as the loading effect. The transient behaviour of this oscillator is simulated using Keysight ADS and the I-V characteristics of the active device was modelled as in (3) with $V_b = 1$ V.

5.1 Start oscillation thresholds

Fig. 7*a* and *b* show one of the main advantages of the double-ladder circuit over a single ladder: An eight-cell double-ladder circuit requires 30% less g_m than an eight-cell single-ladder and 57% less g_m than a 16-cell single-ladder for the circuit to have stable oscillation. In addition, Fig. 7*b* shows the steady-state output voltage amplitude for single- and double-ladder oscillators (both made of 8 unit cells) versus g_m The double-ladder oscillator produces higher load voltage amplitudes, in comparison with the single-ladder counterpart, for small g_m (above threshold) up to $g_m = 2.92$ mS. Above this value, the amplitude of the single ladder becomes higher. However, as g_m keeps increasing, this increases in the amplitude saturates, producing negligible returns for both ladders. The lower oscillation threshold of the double ladder can be attributed to the DBE resonance and the way the voltages and currents are distributed inside the eight-cell structure, which are shown in Figs. 3*c* and *d*. Since the maximum voltage amplitude occurs in the middle of the structure, and the voltage is attenuated by an order of magnitude at the edges, lumped elements that are further away from the middle of the structure have very little effect on the Q_{tot} of the structure, which manifests itself in lower $g_{m,\min}$ to start the oscillation as compared to a single ladder. The obvious implication is that the double-ladder structure has advantages of low-threshold oscillations, specifically in applications requiring low power consumption, while producing diminishing returns for higher values of g_m.

Fig. 7*c* shows the steady-state output voltage amplitude for single- and double-ladder oscillators, with 6 and 8 cells, and all of the inductors and capacitors having half of the quality factor found in [34] and [35], i.e. half of 160 and 210 for 45 and 90 nH inductors, respectively, and half of 460 for the 112 pF capacitor. It is seen from the figure that the double-ladder oscillator always has a lower threshold as compared to an equivalent (in number of cells and Q_e's) single-ladder oscillator. It is observed that the double ladder with 8 cells and half of Q_e's has a lower threshold as compared to a single ladder with only 6 cells and half Q_e's. This is a remarkable since 8 cell double-ladder structure has 40 lossy lumped elements, while 6 cell single ladder has only 12 lossy lumped elements.

5.2 Isolation of the loading effect

One remarkable advantage of the double-ladder oscillator, besides having a lower threshold than the single ladder, is demonstrated in terms of the reduced sensitivity of the oscillation frequency on the load variations. Typically, the oscillation amplitude decreases (and for some cases the oscillator may not even operate) when the output termination resistance is changed from its nominal value. Often, for this reason, the output buffer stages for LC oscillators are needed to isolate it against those variations. Moreover, single-ladder oscillators have been shown to demonstrate *mode jumping* where the oscillation frequency and mode of operation changes for various loads (see for example the analysis in [13], and the explanation of this behaviour in [20] near the band edge). To demonstrate this effect in ladder oscillators, the steady-state load voltage calculated from transient simulations varying as a function of load is considered. The spectrum of the load voltage is then calculated by applying a windowed Fourier transform (rectangular window with width of 1 μs) on the saturated voltage waveform.

The single-ladder load voltage spectrum versus the load resistance, for $g_m = 3$ mS and all elements with $Q_e = 200$ with $N = 8$, is shown in Fig. 8*a*. From this spectrum, it can be seen that the oscillation frequency jumps from the desired frequency near the

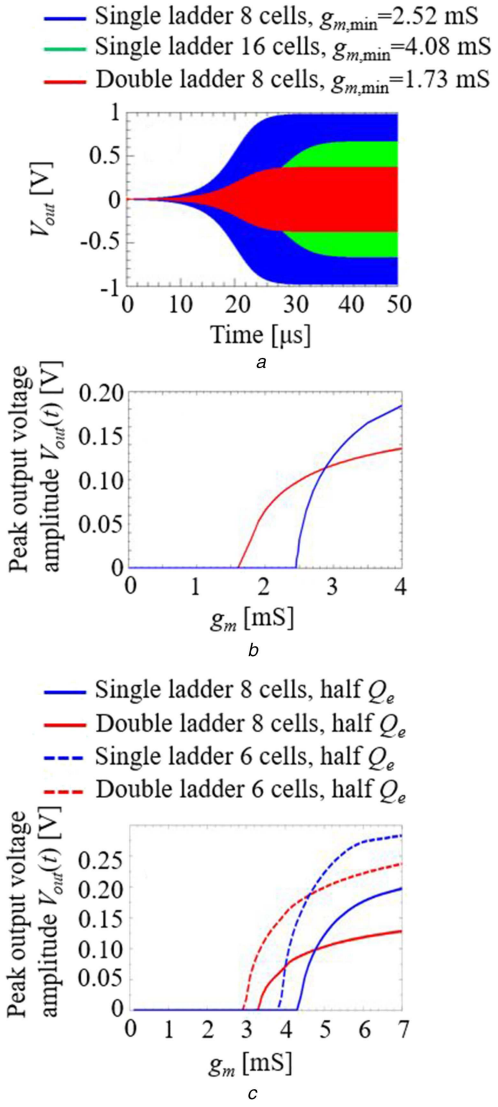

Fig. 7 *Oscillation behavior for single- and double-ladder structures as well as peak output voltage*

(a) Transient load voltage for three different cases of single-ladder and double-ladder oscillators in comparison, ***(b)*** Steady-state output voltage amplitude for different values of g_m comparing single and double ladders with 8 cells with original Q_e's, ***(c)*** Steady-state output voltage amplitude for different values of g_m comparing single and double ladders with 6 and 8 cells, with half of the previously reported Q_e's

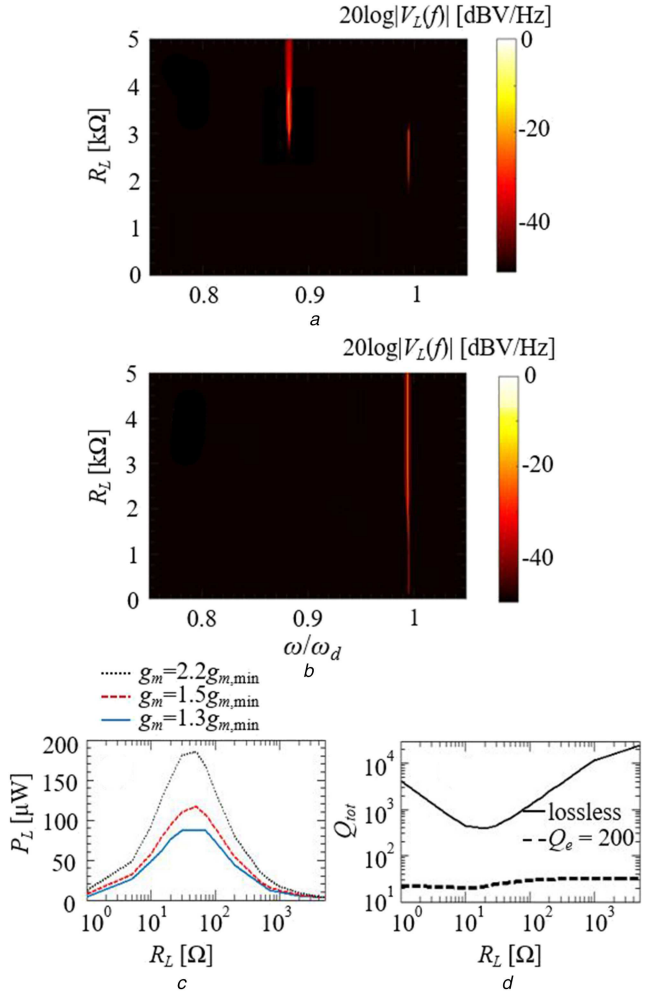

Fig. 8 *Spectrum of load voltage 20log|$V_L(f)$| for*

(a) Single-ladder oscillator, ***(b)*** double-ladder oscillator, both with 8 unit cells, varying as a function of the load resistance R_L, for $g_m = 3$ mS, with all elements with $Q_e = 200$; the plots show the stability of the oscillation frequency of the double-ladder oscillator over a very large variation of the load resistance, ***(c)*** Average steady state power delivered to the load versus loading R_L, for $Q_e = 200$ showing that maximum power is delivered when R_L matches the characteristic impedance of Port 3, ***(d)*** Minimum loaded quality factor corresponding to the lossless double-ladder resonator when varying the load resistance, and almost constant total quality factor considering lossy elements

RBE of the single ladder (~100 MHz) to a lower frequency (~87 MHz) for sufficiently high load impedance. Moreover, this circuit does not oscillate for impedances below 1000 Ω. Indeed, the single ladder threshold for 50 Ω found from Fig. 6*b* confirms that $g_m = 3$ mS is below the threshold for such a load. In contrast, with the double-ladder oscillator with $N = 8$ and $Q_e = 200$, the oscillation frequency is independent of the variation for the load resistance as seen from Fig. 8*b*. Such a remarkable feature of DBE-based oscillators shows the robustness of the design and its resistance to load pulling. The single ladder exhibits multimode oscillation at particular load values (for instance at 3 kΩ the single ladder oscillator can oscillate at both 0.99 ω_d and 0.88 ω_d), instead, the double ladder oscillates at only a single frequency at ~0.995 ω_d demonstrating the unique mode selection scheme of double ladders. Importantly, the double-ladder oscillator also generates the same oscillation frequency for higher values of g_m. These properties can also be observed when the load has a reactive component.

Fig. 8*c* shows the power delivered to the load resistor R_L for three values of g_m above the $g_{m,min}$ and Q_e of 200 for all of the elements. The maximum power delivered to R_L occurs when its value is close to 28 Ω which is the characteristic impedance Z_c of Port 3 of the structure in Fig. 2*a*. Fig. 8*d* is another example of how the double ladder is resistant to load variations. In the lossless case, over a very large range of values of the load resistance, the Q never decreases under a given minimum, and such a minimum has a large Q value. In other words, the plot shows that the Q is large for *any* load resistance in the lossless case. When lumped element losses are considered, Q_{tot} is practically unchanging for a very large range of values of the load resistance.

6 Conclusion and remarks

A novel oscillator concept, based on a periodic double-ladder lumped-element circuit, has been presented in which a DBE condition occurs. The passive behaviour of the double-ladder resonator has been analysed by considering the quality factor scaling over size and effects of loss. It has been shown that the conditions for oscillation are relaxed for the double-ladder as compared to the single-ladder circuit, thus allowing lower power dissipation from the negative conductance circuit that is required. Moreover, the invariability of the oscillation frequency in the presence of variation in the load impedance has been shown to prevent mode-jumping behaviour that can be observed in single ladders. This advantage can result in less power consumption for the active elements.

While the lumped element circuit studied here gives a great foundation for building an oscillator with DBE phenomena, mainly due to the simplicity of the unit cell, it has some limitations that must be considered. One issue that must be considered when implementing this design in the gigahertz frequency range and above, is the decrease of inductor quality factor with increasing frequency, especially in the integrated circuit technology where inductor Q is only 20–30. An obvious workaround the inductor low Q_e limitation is the elimination of all lumped elements by means of implementation of the unit cell with degeneracy condition in another technology, such as microstrip or waveguide where there is no need for lumped elements [14, 16, 43, 44]. As previously mentioned, the simple lumped element structure of this paper already mimics the RF/microwave distributed TL model and, with minor alteration, can easily be translated to a different technology such as TLs, and more specifically microstrip waveguides. We can use microstrip line's inductance and capacitance to avoid the need for realisation of an actual inductor/capacitor and use proximity coupling to imitate the coupling capacitor used in the lumped element design. To avoid a large integration area, equivalent inductance realised by a microstrip line should be as small as current IC technology allows. Since $f_d \propto 1/\sqrt{LC}$, where f_d is the DBE frequency, a compact microstrip design would best be realised at higher RF frequencies since it will not require big inductor and capacitor values. The elimination of all lumped elements from the design, and inductors and capacitors in general, as well as the implementation of the DBE oscillator concept using waveguides, has a potential to be a very power efficient and stable oscillator design based on what discussed here.

Comparison between the proposed double-ladder oscillator and a conventional LC-tank oscillator circuit will be carried out in the future that would account for phase noise, power consumption, and other practical aspects. DBE-based oscillator design may avoid the need for stages of power-hungry current-mode logic buffers to reach acceptable oscillation amplitude at the low impedance termination, as well as improvements to the phase noise.

7 Acknowledgments

This material is based upon work supported by the National Science Foundation under award NSF ECCS-1711975 and by the Air Force Office of Scientific Research under award number FA9550-15-1-0280.

8 References

[1] Moon, Y.-J., Roh, Y.-S., Jeong, C.-Y., *et al.*: 'A 4.39–5.26 GHz LC-tank CMOS voltage-controlled oscillator with small VCO-gain variation', *IEEE Microw. Wirel. Compon. Lett.*, 2009, **19**, (8), pp. 524–526

[2] Ghadiri, A., Moez, K.: 'A dual-band CMOS VCO for automotive radar using a new negative resistance circuitry'. 2010 53rd IEEE International Midwest Symposium on Circuits and Systems (MWSCAS), 2010, pp. 453–456

[3] Razavi, B.: '*Design of integrated circuits for optical communications*' (John Wiley & Sons, New York, NY, 2012)

[4] van der Pol, B.: 'The nonlinear theory of electric oscillations', *Proc. Inst. Radio Eng.*, 1934, **22**, (9), pp. 1051–1086

[5] Pierce, G.W.: 'Piezoelectric crystal resonators and crystal oscillators applied to the precision calibration of wavemeters'. Proc. of the American Academy of Arts and Sciences, 1923, vol. 59, pp. 81–106

[6] Colpitts, E.H.: United States Patent No. US1624537A. Retrieved from https://patents.google.com/patent/US1624537A/en, 1927

[7] Collin, R.E.: '*Foundations for microwave engineering*' (John Wiley & Sons, New York, NY, 2007)

[8] Wu, H., Hajimiri, A.: 'Silicon-based distributed voltage-controlled oscillators', *IEEE J. Solid-State Circuits*, 2001, **36**, (3), pp. 493–502

[9] Tanaka, H.-A., Hasegawa, A., Mizuno, H., *et al.*: 'Synchronizability of distributed clock oscillators', *IEEE Trans. Circuits Syst. Fundam. Theory Appl.*, 2002, **49**, (9), pp. 1271–1278

[10] Hajimiri, A., Limotyrakis, S., Lee, T.H.: 'Jitter and phase noise in ring oscillators', *IEEE J. Solid-State Circuits*, 1999, **34**, (6), pp. 790–804

[11] Nayak, R., Kianpoor, I., Bahubalindruni, P.G.: 'Low power ring oscillator for IoT applications', *Analog Integr. Circuits Signal Process.*, 2017, **93**, (2), pp. 1–7

[12] Chang, H.-C., Cao, X., Mishra, U.K., *et al.*: 'Phase noise in coupled oscillators: theory and experiment', *IEEE Trans. Microw. Theory Tech.*, 1997, **45**, (5), pp. 604–615

[13] Endo, T., Mori, S.: 'Mode analysis of a multimode ladder oscillator', *Circuits Syst. IEEE Trans.*, 1976, **23**, (2), pp. 100–113

[14] Löcker, C., Sertel, K., Volakis, J.L.: 'Emulation of propagation in layered anisotropic media with equivalent coupled microstrip lines', *IEEE Microw. Wirel. Compon. Lett.*, 2006, **16**, (12), pp. 642–644

[15] Volakis, J.L., Sertel, K.: 'Narrowband and wideband metamaterial antennas based on degenerate band edge and magnetic photonic crystals', *Proc. IEEE*, 2011, **99**, (10), pp. 1732–1745

[16] Othman, M., Capolino, F.: 'Demonstration of a degenerate band edge in periodically-loaded circular waveguides', *IEEE Microw. Wirel. Compon. Lett.*, 2015, **25**, (11), pp. 700–702

[17] Othman, M.A.K., Pan, X., Atmatzakis, Y., *et al.*: 'Experimental demonstration of degenerate band edge in metallic periodically-loaded circular waveguide', *IEEE Microw. Theory Tech.*, 2017, **1611**, (8), p. 9

[18] Othman, M.A., Veysi, M., Figotin, A., *et al.*: 'Low starting electron beam current in degenerate band edge oscillators', *IEEE Trans. Plasma Sci.*, 2016, **44**, (6), pp. 918–929

[19] Veysi, M., Othman, M.A.K., Figotin, A., *et al.*: 'Degenerate band edge laser', *Phys. Rev. B*, 2018, **97**, (19), p. 195107

[20] Sloan, J.T., Othman, M.A.K., Capolino, F.: 'Theory of double ladder lumped circuits with degenerate band edge', *IEEE Trans. Circuits Syst. I, Regul.Pap.*, 2018, **65**, (1), pp. 3–13

[21] Felsen, L.B., Kahn, W.K.: 'Transfer characteristics of 2n-port networks'. Proc. of the Symp. on Millimeter Waves, 1959, (Published by Polytechnic Press., New York, Brooklyn, 1960) pp. 477–512

[22] Figotin, A., Vitebskiy, I.: 'Gigantic transmission band-edge resonance in periodic stacks of anisotropic layers', *Phys. Rev. E*, 2005, **72**, (3), p. 036619

[23] Tamma, V.A., Figotin, A., Capolino, F.: 'Concept for pulse compression device using structured spatial energy distribution', *IEEE Trans. Microw. Theory Tech.*, 2016, **64**, (3), pp. 742–747

[24] Matthaei, G.L., Young, L., Jones, E.M.: 'Design of microwave filters, impedance-matching networks, and coupling structures. Volume 2'. DTIC Document, 1963

[25] Zverev, A.I.: '*Handbook of filter synthesis*' (Wiley, New York, NY, 1967)

[26] Williams, A.B., Taylor, F.J.: '*Electronic filter design handbook*' (McGraw-Hill Inc., New York, NY, 1995)

[27] Pozar, D.M.: '*Microwave engineering*' (John Wiley & Sons, New York, NY, 2009)

[28] Joannopoulos, J.D., Johnson, S.G., Winn, J.N., *et al.*: '*Photonic crystals: molding the flow of light*' (Princeton University Press, Princeton, NJ, 2011)

[29] Bahr, A.J.: 'A coupled-monotron analysis of band-edge oscillations in high-power traveling-wave tubes', *IEEE Trans. Electron. Devices*, 1965, **12**, (10), pp. 547–556

[30] Kuznetsov, A.P., Kuznetsov, S.P., Rozhnev, A.G., *et al.*: 'Wave theory of a traveling-wave tube operated near the cutoff', *Radiophys. Quantum Electron.*, 2004, **47**, (5–6), pp. 356–373

[31] Dowling, J.P., Scalora, M., Bloemer, M.J., *et al.*: 'The photonic band edge laser: a new approach to gain enhancement', *J. Appl. Phys.*, 1994, **75**, (4), pp. 1896–1899

[32] Ryu, H.-Y., Kwon, S.-H., Lee, Y.-J., *et al.*: 'Very-low-threshold photonic band-edge lasers from free-standing triangular photonic crystal slabs', *Appl. Phys. Lett.*, 2002, **80**, (19), pp. 3476–3478

[33] Othman, M.A.K., Yazdi, F., Figotin, A., *et al.*: 'Giant gain enhancement in photonic crystals with a degenerate band edge', *Phys. Rev. B*, 2016, **93**, (2), p. 024301

[34] 'http://www.coilcraft.com'. Available at http://www.coilcraft.com

[35] 'http://www.avx.com/'. Available at http://www.avx.com/

[36] Apaydin, N., Zhang, L., Sertel, K., *et al.*: 'Experimental validation of frozen modes guided on printed coupled transmission lines', *IEEE Trans. Microw. Theory Tech.*, 2012, **60**, (6), pp. 1513–1519

[37] Burr, J.R., Gutman, N., Martijn de Sterke, C., *et al.*: 'Degenerate band edge resonances in coupled periodic silicon optical waveguides', *Opt. Express*, 2013, **21**, (7), pp. 8736–8745

[38] Lee, T.H., Hajimiri, A.: 'Oscillator phase noise: a tutorial', *IEEE J. Solid-State Circuits*, 2000, **35**, (3), pp. 326–336

[39] Leeson, D.B.: 'A simple model of feedback oscillator noise spectrum', *Proc. IEEE*, 1966, **54**, (2), pp. 329–330

[40] Craninckx, J., Steyaert, M.: 'Low-noise voltage-controlled oscillators using enhanced LC-tanks', *IEEE Trans. Circuits Syst. II Analog Digit. Signal Process.*, 1995, **42**, (12), pp. 794–804

[41] Jung, B., Harjani, R.: 'ΣHigh-frequency LC VCO design using capacitive degeneration', *IEEE J. of Solid-State Circuits*, 2004, **39**, (12), pp. 2359–2370

[42] Skogestad, S., Postlethwaite, I.: '*Multivariable feedback control: analysis and design*' vol. **2,** (Wiley, New York, 2007)

[43] Othman, M.A., Capolino, F.: 'Theory of exceptional points of degeneracy in uniform coupled waveguides and balance of gain and loss', *IEEE Trans. Antennas Propag.*, 2017, **65**, (10), pp. 5289–5302

[44] Abdelshafy, A.F., Othman, M.A.K., Oshmarin, D., *et al.*: 'Exceptional points of degeneracy in periodically-coupled waveguides and the interplay of gain and radiation loss: theoretical and experimental demonstration', *ArXiv180905256 Phys.*, 2018